



**HAL**  
open science

## The aminosterol Claramine inhibits $\beta$ -secretase 1-mediated insulin receptor cleavage

Bénédicte Gaborit, Roland Govers, Alexandre Altié, Jean Michel Brunel,  
Pierre Morange, Franck Peiretti

### ► To cite this version:

Bénédicte Gaborit, Roland Govers, Alexandre Altié, Jean Michel Brunel, Pierre Morange, et al.. The aminosterol Claramine inhibits  $\beta$ -secretase 1-mediated insulin receptor cleavage. *Journal of Biological Chemistry*, 2021, 297 (1), pp.100818. 10.1016/j.jbc.2021.100818 . hal-03368302

**HAL Id: hal-03368302**

**<https://hal.science/hal-03368302>**

Submitted on 11 Oct 2021

**HAL** is a multi-disciplinary open access archive for the deposit and dissemination of scientific research documents, whether they are published or not. The documents may come from teaching and research institutions in France or abroad, or from public or private research centers.

L'archive ouverte pluridisciplinaire **HAL**, est destinée au dépôt et à la diffusion de documents scientifiques de niveau recherche, publiés ou non, émanant des établissements d'enseignement et de recherche français ou étrangers, des laboratoires publics ou privés.



Distributed under a Creative Commons Attribution 4.0 International License

## **The aminosterol Claramine inhibits $\beta$ -secretase 1-mediated insulin receptor cleavage**

Bénédicte Gaborit<sup>1,2</sup>, Roland Govers<sup>1</sup>, Alexandre Altié<sup>1</sup>, Jean Michel Brunel<sup>3</sup>, Pierre Morange<sup>1,4</sup>, Franck Peiretti<sup>1\*</sup>

<sup>1</sup>Aix Marseille University, INSERM, INRAE, C2VN, 13385 Marseille, France.

<sup>2</sup>Endocrinology, Metabolic Diseases and Nutrition Department, APHM, 13005 Marseille, France.

<sup>3</sup>Aix Marseille University, INSERM, SSA, MCT, 13385 Marseille, France.

<sup>4</sup>Hematology Laboratory, La Timone Hospital, APHM, 13385 Marseille, France.

\*Correspondence: franck.peiretti@univ-amu.fr

Franck Peiretti: ORCID iD: 0000-0001-7198-0534

**Running title:** Insulin receptor cleavage

**Keywords:** Insulin receptor, beta-secretase 1 (BACE1), liver, diabetes, O-GlcNacylation, proteasome, lysosome, autophagy

## Abstract

The cleavage of the insulin receptor by  $\beta$ -secretase 1 (BACE1) in the liver increases during diabetes, which contributes to reduce insulin receptor levels and impair insulin signaling. However, the precise signaling events that lead to this increased cleavage are unclear. We showed that BACE1 cleaves the insulin receptor in the early secretory pathway. Indeed, co-immunoprecipitation experiments reveal the interaction of the proforms of the two proteins. Moreover, fragments of insulin receptor are detected in the early secretory pathway and a mutated form of BACE1 that retains its prodomain cleaves an early secretory pathway-resident form of the insulin receptor. We showed that BACE1 proform levels are regulated by proteasome and/or lysosome-dependent degradation systems whose efficiencies are dependent on the *O*-GlcNacylation process. Our results showed that enhanced *O*-GlcNacylation reduces the efficiency of intracellular protein degradation systems, leading to the accumulation of the proform of BACE1 in the early secretory pathway where it cleaves the precursor of the insulin receptor. All these dysregulations are found in the livers of diabetic mice. In addition, we performed a screen of molecules according to their ability to increase levels of the insulin receptor at the surface of BACE1 overexpressing cells. This approach identified the aminosterol Claramine, which accelerated intracellular trafficking of the proform of BACE1 and increased autophagy. Both of these effects likely contribute to the reduced amount of the proform of BACE1 in the early secretory pathway, thereby reducing insulin receptor cleavage. These newly described properties of Claramine are consistent with its insulin sensitizing effect.

## Introduction

The insulin receptor (IR) mediates the metabolic and mitogenic effects of insulin. Dysfunctions in insulin signaling are responsible for the metabolic syndrome and type 2 diabetes (1) but are also implicated in a variety of cancers (2,

3) and increasingly associated with neurodevelopmental disorders (4, 5).

The decreased IR tyrosine kinase activity with reduction in post-receptor signaling is one of the causes of insulin signaling dysfunction. This aspect has been studied relentlessly for decades and progress in this area is regularly and comprehensively reviewed (6). IR content reduction has long been suspected to contribute to the defective insulin signaling and diabetes progression. This has been firmly proven by showing that restoring IR expression in the liver of adult diabetic mouse models improves the diabetic phenotypes (7). Moreover, studies have demonstrated that mechanisms regulating density of cell surface functional IR have significant effects on insulin cell signaling. In this line, it was reported that E3 ubiquitin ligases MARCH1 in liver (8) or mitsugumin 53 in muscle (9) impaired insulin action by targeting cell surface IR for ubiquitin-dependent degradation, resulting in a reduction of its cell surface density. In liver, IR cell surface internalization, controlled by the module p31<sup>comet</sup>-MAD2-BUBR1, was shown to be a mechanism regulating insulin signaling (10). In adipocytes, redirection of internalized IR from endosomes to the plasma membrane, controlled by the intracellular sorting receptor SORLA, regulates IR cell surface expression and insulin signaling (11). We have previously established that IR ectodomain is cleaved by BACE1 (12). This cleavage occurs in the liver and increases during diabetes, thus reducing the density of functional IR on the cell surface. Interestingly, BACE1 inhibition restores functional cell-surface IR and increases insulin signaling, making the liver BACE1-dependent IR cleavage regulation system an original target for counteracting impaired insulin signaling. The purpose of this study was to elucidate the mechanisms that regulate BACE1-

dependent cleavage of IR during diabetes to identify regulatory steps that could be pharmacologically targeted to reduce IR cleavage and improve insulin sensitivity.

## Results

### **BACE1-dependent cleavage of IR occurs in the early secretory pathway**

Our previous results suggested that BACE1 zymogen (proBACE1, with its prodomain) was responsible for IR cleavage. This possibility was thoroughly investigated below.

In lysates of cells expressing FLAG-tagged IR and HA-tagged BACE1, IR precursor (proIR composed of a single polypeptide chain) and mature IR (derived from the cleavage of proIR by furin and yielding the  $\alpha$  and  $\beta$  subunits of IR) (Supporting Fig. S1) were detected with the antibody specific for the C-terminal region of IR (Fig. 1a). proBACE1 was detected by the antibody specific for BACE1 prodomain (below 60 kDa), while HA tag antibodies detected a form of BACE1 that migrates slower than proBACE1 (around 60kDa) that likely corresponds to mature BACE1 (without its prodomain but with its complex glycans moiety) (Fig. 1a). Once immunoprecipitated BACE1 was detected by immunoblot as two major distinct bands (Fig. 1b): the lowest one corresponding to proBACE1, since it was also detected by the antibody specific for BACE1 prodomain, the upper one being the mature BACE1. A 100 kDa HA-tagged protein was also detected. proBACE1 and the 100 kDa HA-tagged protein co-immunoprecipitated with IR and were both detected with BACE1 prodomain specific antibodies (Fig. 1b). Interestingly, overexpression of the proprotein convertase (PC) furin, that increases the cleavage of BACE1 propeptide (13), reduced the detection of proBACE1 and that of the 100 kDa protein (Fig. 1c) while allowing the detection of a HA-tagged

protein that migrated slightly above 100 kDa. These features suggest that the 100 kDa protein is a high-molecular weight form of proBACE1 and that the protein above 100 kDa, detected upon furin overexpression, is a high-molecular weight form of mature BACE1. The nature of the 100 kDa proBACE1 was investigated by co-immunoprecipitation of overexpressed HA-tagged BACE1 and FLAG-tagged BACE1. Immunoprecipitation of FLAG-BACE1 pulled down the proform of HA-BACE1 and that of 100 kDa HA-tagged BACE1 (Fig. 1d), suggesting that proBACE1 is expressed in cells in a non-monomeric form and that the 100 kDa high-molecular weight form of proBACE1 is a reduction and SDS-resistant dimer of proBACE1. Likewise, the high-molecular weight form of BACE1 detected upon furin overexpression (Fig. 1c) is likely a dimer of mature BACE1. In addition, immunoprecipitation of BACE1 mostly pulled down proIR (Fig. 1e). These results support that proIR interacts with monomeric and/or dimeric proBACE1. However, this interaction does not necessarily imply that proBACE1 is responsible for IR cleavage. To address this concern, we generated BACE1<sub>R42G</sub> that resists PC-induced maturation as shown by the detection of a slow migrating form of proBACE1 (Fig. 2a), which likely corresponds to proBACE1 that crossed the Golgi stack and acquired its complex N-glycosylation, as previously demonstrated (14). BACE1<sub>R42G</sub> and wild-type BACE1 were similarly effective in cleaving IR as shown by the release of soluble IR (IR<sub>SOL</sub>) in the culture media (Fig. 2a) and the generation of the transmembrane IR C-terminal fragment (IR<sub>CTF</sub>) (Fig. 2b). By comparison, small amounts of IR<sub>SOL</sub> and IR<sub>CTF</sub> were generated when the inactive BACE1<sub>D289A</sub> was overexpressed. IR<sub>CTF</sub> is normally cleaved by the  $\gamma$ -secretase, which generates an unstable fragment of its

intracellular domain ( $IR_{ICD}$ ) that is rapidly degraded by the proteasome; therefore, inhibition of  $\gamma$ -secretase with DAPT is mandatory to observe an  $IR_{CTF}$  that best reflects the BACE1-dependent cleavage of IR (Supporting Fig. S1). With respect to other BACE1 substrates: Neuregulin1 (NRG1) was less effectively cleaved by BACE1<sub>R42G</sub> than by wild-type BACE1, while the amyloid precursor protein (APP) and its mutated form APP<sub>swe</sub> were similarly cleaved by both BACE1 forms (Supporting Fig. S2a). These results show that IR cleavage does not necessarily require the PC-dependent maturation of proBACE1, but they do not rule out that mature BACE1 may also cleave IR.

The cleavage of IR by proBACE1 implies that it takes place in the early secretory pathway (ESP), from endoplasmic reticulum (ER) and before the trans Golgi network (TGN) where the PC cleaves BACE1 prodomain, whereas mature BACE1 would cleave IR from TGN and beyond. We therefore analyzed the BACE1-dependent cleavage of IR mutated forms that are sequestered in the ESP. We have previously described the ESP sequestration of an IR mutated form that resists BACE1 cleavage, in which amino acids flanking the scissile bond are substituted (F<sub>942</sub>K/Y<sub>943</sub>K giving  $IR_{FY/KK}$ ) (12). Figure 2C confirms the ESP retention of  $IR_{FY/KK}$  (mainly  $IR_{FY/KK}$  precursor was detected) and its resistance to BACE1 cleavage (small amount of  $IR_{CTF}$  was detected). The construct  $IR_{FY/AA}$  was also retained in the ESP but, unlike  $IR_{FY/KK}$ , it was effectively cleaved by BACE1 as significant amounts of  $IR_{CTF}$  (Fig. 2c) and  $IR_{SOL}$  (Fig. 2d) were generated. These results support that BACE1 can cleave IR in ESP where both proteins exist in their precursor forms. They also imply the existence of a N-terminal fragment of proIR ( $IR_{NTF}$ ) contained in intracellular vesicles, which once secreted is identified

as  $IR_{SOL}$  (Supporting Fig. S1). In lysates of active BACE1 expressing cells, anti- $IR_{\alpha}$  subunit antibodies detected a protein below the position of  $IR_{FY/AA}$  precursor, suggesting that this protein is the BACE1-generated  $IR_{NTF}$  (Fig. 2c and 2d). SDS-PAGE migration distances of  $IR_{FY/AA}$  precursor and its  $IR_{NTF}$  were increased by EndoH treatment of the cell lysates (Fig. 2e), which removes glycans from core glycosylated proteins that have not trafficked to the cis-medial Golgi apparatus, showing that these two proteins are present within the ESP.

The  $IR_{NTF}$  generated in ESP cisternae should be a single polypeptide chain consisting of the entire  $IR_{\alpha}$  subunit and a fragment of the  $IR_{\beta}$  subunit which, once in the TGN,  $IR_{NTF}$  should be cleaved by PC (Supporting Fig. S1). Inhibition of PC (by EK4 overexpression (15) or pharmacological treatment) reduced the proteolytic maturation of IR (increased amount of proIR, decreased amount of  $IR_{\beta}$ ) and BACE1 (increased detection of proBACE1) but did not impair the BACE1-dependent cleavage of IR as judged by the detection of  $IR_{CTF}$  and  $IR_{SOL}$  (Fig. 2f). However,  $IR_{SOL}$  generated under PC inhibition showed a reduced mobility on SDS-PAGE which is consistent with an  $IR_{NTF}$  that is not cleaved by PC.

Interestingly, fractionation of the subcellular membrane vesicles of HepG2 hepatoma cells by iodixanol density gradient ultracentrifugation allowed the detection of proIR,  $IR_{CTF}$  and  $IR_{NTF}$  in the Golgi apparatus and ER-enriched fractions (Fig. 2g), suggesting that cleavage of endogenous IR occurs in ESP. However, as expected for transmembrane proteins transported through the secretory pathway,  $IR_{CTF}$  and  $IR_{\beta}$  have similar sedimentation profiles.  $IR_{NTF}$ , which is an intravesicular fragment of proIR, was narrowly detected in Golgi apparatus and ER-enriched fractions.

Taken together, these results provide arguments in favor of a cleavage of proIR by proBACE1 that occurs in ESP.

### **Degradation-dependent regulation of proBACE1 amount**

We have previously observed that proBACE1 amount and IR cleavage were regulated by the glucose concentration of the cell culture media and we have suggested that the hexosamine biosynthetic pathway (HBP) plays a key role of in this process (12). In agreement with this proposal, proBACE1 amount was reduced when cells were incubated in low glucose media, an effect prevented by the addition of the HBP substrate glucosamine (Fig. 3a). Furthermore, low glucose media or reduction of *O*-GlcNAcylation by inhibiting either L-Glutamine-D-fructose 6-phosphate amidotransferase (the HBP rate-limiting enzyme) by DON or *O*-GlcNAc transferase (the enzyme that attaches a GlcNAc moiety on specific proteins) by OSMI-1 (16), reduced global *O*-GlcNAcylation and decreased the amount of proBACE1 without major alterations of the amount of mature BACE1 (Fig. 3b). These results confirm that *O*-GlcNAcylation controls proBACE1 proteostasis. We therefore investigated the mechanisms responsible for proBACE1 degradation.

proBACE1 amount was increased by treatment of cells with inhibitors of lysosome-dependent proteolysis, which increased the accumulation of the autophagosomes marker LC3II, and by inhibitors of proteasome-dependent proteolysis, which increased the accumulation of ubiquitinated proteins (Fig. 3c). Bafilomycin A1 (BAF; a V-ATPase inhibitor that increases lysosomal pH preventing lysosomal proteases activity) and MG132 (which blocks the proteolytic activity of the 26S proteasome complex) were used for the remainder of the study. Both inhibitors increased proBACE1 levels

and less markedly those of mature BACE1 (Fig. 3c and 3d). Comparatively, these inhibitors poorly altered the amount of precursor and mature IR (Fig. 3d). proBACE1 stable dimer was also increased by BAF and MG132 treatment (Fig. 3c, 3d and 5a). Importantly, treatment of HepG2 hepatoma cells with BAF increased the amount of endogenous proBACE1 (Fig. 3e and Supporting Fig. S4b), indicating that the regulation observed with over-expressed BACE1 is valid for endogenous BACE1. In HepG2 cells, endogenous proBACE1 was poorly expressed and its detection required its preliminary enrichment by heparin-agarose-based affinity chromatography, as previously described (17). These results demonstrate that the amount of proBACE1 contained in ESP is regulated by proteasome- and/or lysosome-dependent proteolysis, implying the involvement of ER-associated degradation (ERAD) and/or ER-to-lysosome-associated degradation (ERLAD) pathways (18, 19) (thereafter abbreviated as ER(L)AD).

### **Ubiquitin-independent degradation of proBACE1**

BACE1 was previously shown to be ubiquitinated at lysine 501 (20). We therefore analyzed the involvement of this post-translational modification (PTM) in the regulation of proBACE1 degradation. Basal expression of proBACE1 and proBACE1<sub>K501R</sub> (that cannot be ubiquitinated) were similar (Fig. 4a) and ubiquitin overexpression, which leads to the accumulation of ubiquitinated proteins that overloads the degradation systems and slows down proteolysis, greatly increased the amounts of proBACE1 and proBACE1<sub>K501R</sub> and minimally those of total BACE1 (Fig. 4a). Immunoprecipitation of BACE1 followed by ubiquitin detection confirmed the ubiquitination of BACE1 at Lysine 501 by

K63-linked polyubiquitin chains (Fig. 4b) and immunoprecipitation of FLAG-tagged ubiquitin followed by the detection of proBACE1 revealed the ubiquitination of proBACE1 (Fig. 4b). Therefore, our results are in favor of a K63-linked ubiquitination of pro and mature BACE1. BACE1 lysine 501 was also shown to be a site for SUMO1 conjugation (21). However, our results are not in favor of incorporation of the non-deconjugatable SUMO1<sub>Q89P</sub> into BACE1 (Supporting Fig. S3).

Basal levels of pro and total BACE1 and BACE1<sub>K501R</sub> were comparable and were similarly increased by inhibition of lysosome- or proteasome-dependent proteolysis (Fig. 4c). Furthermore, IR was similarly cleaved by overexpressed BACE1 and BACE1<sub>K501R</sub> as judged by the generation of IR<sub>CTF</sub> (Fig. 4d) and the release of IR<sub>SOL</sub> (Fig. 4e). The IR cleavage was distinctly affected by treatment with BAF, indeed the IR<sub>CTF</sub> was reduced (Fig. 4d), however, IR<sub>SOL</sub> remained unchanged (Fig. 4e).

Therefore, PTM of BACE1 at lysine 501 is not involved in the regulation of proBACE1 levels by the two major types of protein degradation pathways. These results support the ubiquitin-independent degradation of proBACE1 by ER(L)AD systems.

### **ER stress regulates proBACE1 amount**

The involvement of ER(L)AD in proBACE1 proteostasis suggests that proBACE1 amount may be regulated by ER stress.

In addition to increasing proBACE1 levels, inhibition of ER(L)AD systems by treatment with BAF or MG132 allowed the accumulation of ubiquitin-conjugated proteins (Fig. 5a) that can ultimately trigger ER stress. Coherently, BAF and MG132 increased mRNA levels of ER stress markers (Fig. 5b). The increase in proBACE1 levels and ubiquitin-conjugated protein accumulation triggered by BAF

and MG132 were partially prevented by simultaneous treatment with OSMI-1 (Fig. 5a), which decreases O-GlcNacylation. Interestingly, OSMI-1 also prevented the increase in mRNA levels of the ER stress markers GRP78 and sXBP1 induced by BAF but not by MG132 (Fig. 5b) and reduced the amount of GRP78 protein under basal and BAF-treated conditions (Fig. 5a). Remarkably, CHOP mRNA levels were not altered by OSMI-1 treatment (Fig. 5b).

These results suggest that ER(L)AD (probably more specifically ERLAD), O-GlcNacylation process, ER stress and the regulation of proBACE1 amount are somehow functionally interrelated. In favor of this interpretation, treatment of cells with the ER stress inducer A23187 (22) upregulated the expression of ER stress markers (Fig. 5c) and increased the amount of proBACE1 (Fig. 5d).

### **Regulation of proBACE1 in the liver of diabetic mouse models**

Global protein O-GlcNacylation and ubiquitination were increased in liver of mice fed a high-fat diet (HFD) compared to standard-fat diet-fed (SFD) mice (Fig. 6a) as well as in those from *db/db* mice compared with their control (*db/+*) littermates (Fig. 6b). ER stress was increased in livers of HFD fed mice and *db/db* mice, as indicated by the increased mRNA levels of some ER stress markers (Fig. 6c) and reduced amount of GRP78 protein (Fig. 6b), respectively. Therefore, the regulatory events that control the amount of proBACE1 (O-GlcNacylation, ER(L)AD and ER stress) are disturbed in the liver of mouse models of diabetes. As expected, the amount of proBACE1 was increased in the liver of *db/db* mice (Fig. 6b and Supporting Fig. S4a and S4b), which is in accordance with the increased BACE1 expression (12) (Fig. 6d and Supporting Fig. S4c).

### **Claramine reduces BACE1-dependent cleavage of IR**

Previously produced aminosterol compounds (23) (Supporting Fig. S5a) were screened for their ability to increase the expression of IR on the surface of cells overexpressing BACE1. To that end, luminescence generated by the previously described “IR cleavage reporter system” (12) was measured on the surface of cells expressing BACE1 (Supporting Fig. S5b). The most important increase in cell surface-associated luminescence was obtained with Claramine treatment (Supporting Fig. S5c). In agreement with this result, Claramine increased the amount of IR on the surface of cells expressing BACE1 but not on the surface of cells expressing inactive BACE1<sub>D289A</sub> (Fig. 7a and Supporting Fig. S5d). In addition, Claramine reduced the generation of IR<sub>CTF</sub> (Fig. 7b) and decreased the amount of IR<sub>SOL</sub> accumulated in the conditioned media of BACE1-overexpressing cells (Fig. 7c). The small magnitude of IR<sub>SOL</sub> reduction is likely due in part to the fact that Claramine increases the BACE1-independent IR release, as observed in the conditioned media of inactive BACE1<sub>D289A</sub>-overexpressing cells (Fig. 7c). These results suggest that the inhibition of proBACE1-dependent cleavage of IR by Claramine is responsible for the increased amount of cell surface IR. Knockdown experiments, previously demonstrated that endogenous IR is cleaved by endogenous BACE1 (12) in HepG2 hepatoma cells. Interestingly, treatment of these cells with Claramine reduced cellular accumulation of IR<sub>CTF</sub> (Supporting Fig. S5e) and increased cell surface expression of IR (Supporting Fig. S5f), implying that endogenous IR cleavage can be reduced by Claramine. Importantly, Claramine decreased the amount of APP and APP<sub>swe</sub> C-terminal fragments (Supporting Fig. S2b), suggesting that it reduces their cleavage

and therefore that BACE1 is the target of Claramine action. In contrast, Claramine decreased the total amount of NRG1 (full-length and C-terminal fragment) (Supporting Fig. S2b), which is not consistent with a reduction of its cleavage. Claramine increased the amount of complex N-glycosylated proBACE1 (Fig. 7d and Supporting Fig. S6a) but did not affect proIR (Fig. 7b), suggesting that Claramine increases the transport of proBACE1 to the Golgi apparatus without excessive impairment of overall vesicular trafficking. In addition, Claramine reduced the amount of core glycosylated proBACE1 (Fig. 7d and Supporting Fig. S6a), an effect particularly pronounced when proteasome was inhibited (Fig. 7d), and which suggests that Claramine activates proBACE1 lysosomal-dependent degradation. In agreement with this, Claramine increased autophagy in HepG2 cells as demonstrated by the decreased accumulation of LC3-HiBiT reporter (Fig. 7e), the increase in the amount of LC3II and LC3II/LC3I ratio (Fig. 7f) (also observed in HEK293 cells, Supporting Fig. S6), and the formation of autophagosomes (Fig. 7g). Importantly, inhibition of early-stage autophagy by LY294002 (24, 25) increased the amount of proBACE1 (Fig. 7h), which is consistent with the involvement of autophagy in proBACE1 regulation. Remarkably, the autophagy inducer Resveratrol (26) did not increase the transport of proBACE1 to the Golgi apparatus (Supporting Fig. S6), ruling out that Claramine-induced activation of proBACE1 trafficking is solely due to the increase in autophagy it triggers.

We have previously shown that the insulin-stimulated expression of immediate-early gene *EGR1* was proportional to the amount of functional IR (12). In agreement, *EGR1* promoter activity was higher in inactive BACE1<sub>D289A</sub> expressing cells than in wild-type BACE1

expressing cells (Supporting Fig. S7a). We therefore measured the activity of *EGR1* promoter to evaluate whether the Claramine-induced increase in cell surface IR could enhance insulin response. When functional IR was expressed, Claramine increased basal and insulin-stimulated transcription of *EGR1* with similar amplitudes whether cells expressed wild-type BACE1 or inactive BACE1<sub>D289A</sub>, while no effect was observed when the kinase dead IR<sub>Y3F</sub> was expressed (Supporting Fig. S7a). These results suggest that Claramine directly stimulates IR signaling, which was further confirmed by showing that Claramine increased IR autophosphorylation (Supporting Fig. S7b). Interestingly, IGF1R autophosphorylation was not increased by Claramine (Supporting Fig. S7b).

## Discussion

Mechanisms that regulate the cleavage of IR by BACE1 in the liver during diabetes may constitute targets to improve insulin sensitivity. Our results demonstrate that the decrease in ER(L)AD activity triggers the accumulation of proBACE1 in ESP which leads to proIR cleavage. This cascade of reactions, which can be initiated by an increased *O*-GlcNacetylation, is reversed by Claramine (Fig. 8).

We have compiled arguments demonstrating that proBACE1 can cleave proIR in the ESP. First: proBACE1 interacts with proIR. Second: lowering PC activity reduces BACE1 and IR maturation without decreasing BACE1-dependent IR cleavage; in agreement BACE1<sub>R42G</sub>, that cannot be proteolytically matured by PC, still cleaves IR. Third: IR<sub>FY/AA</sub> that resides in ESP as precursor form is cleaved by BACE1 and BACE1<sub>R42G</sub>. Fourth: IR<sub>NTF</sub> is generated by BACE1 in ESP (as attested by its sensitivity to EndoH deglycosylation). Fifth: endogenous IR<sub>NTF</sub> co-sediments with the Golgi apparatus and the ER during

fractionation of subcellular membrane vesicles. The ability of proBACE1 to cleave APP in ESP has already been described (13, 27) and we confirm that the presence of the prodomain in BACE1<sub>R42G</sub> does not markedly alter APP and APP<sub>swe</sub> cleavage. On the opposite, NRG1 is less cleaved by BACE1<sub>R42G</sub> than by BACE1, showing that the cleavage of specific substrates can be hindered by the presence of BACE1 prodomain. We detected a dimeric form of proBACE1 that interacts with IR and whose amount seems proportional to the amount of proBACE1 in the ESP. Interestingly, it was proposed that BACE1 dimerization would facilitate binding and cleavage of physiological substrates (28). We have highlighted the involvement of *O*-GlcNacetylation process in the regulation of proBACE1 amount. *O*-GlcNacetylation is known to control proteasome activity (29, 30) and autophagic flux (31, 32). Our results confirm these findings since inhibition of *O*-GlcNacetylation reduces global protein ubiquitination in basal situation and upon inhibition of proteasome or lysosome/autophagy. We propose that, when lysosome/autophagy is inhibited, a reduction in *O*-GlcNacetylation increases proteasomal degradation; inversely, when proteasome activity is inhibited, the reduced *O*-GlcNacetylation stimulates degradation lysosomal-dependent degradation. This interpretation is consistent with the prevailing theory that considers proteasome and autophagy as two complementary and mutually regulated protein degradation systems (33). Importantly, inhibition of proteasome- or lysosome/autophagy-dependent degradations induces a substantial increase in proBACE1 amount, which is prevented by inhibition of *O*-GlcNacetylation. The involvement of proteasome (34–36) or lysosome (20, 37) in the regulation of BACE1 degradation

has already been reported. Interestingly, increased amounts of proBACE1 were observed when Ubiquitin carboxyl-terminal hydrolase L1 is knocked down (38) or when lysosome is inhibited (37). Therefore, our results showing that proteasome or lysosome inhibition increases the amount of proBACE1 are consistent with these earlier unexplained observations. In addition, we show that an inhibitor of early-stage autophagy increases proBACE1 amount, suggesting a direct role of autophagy in this regulation. K48-linked polyubiquitin chain has been shown to be sufficient to target substrates to the 26S proteasome while K63-linked polyubiquitin chain is involved in various stages of internalization, lysosome sorting and degradation processes of membrane proteins (39, 40). However, this concept is oversimplified and exceptions occur. For instance, both K63 and K48 ubiquitin linkages signal lysosomal degradation of the LDL receptor (41). We confirm that BACE1 is ubiquitinated at Lysine 501 by K63-linked polyubiquitin chain (20) and show that proBACE1 is also subject to this PTM. There is no consensus regarding the stability of the ubiquitination-deficient BACE1<sub>K501R</sub>: it was shown to behave like wild-type BACE1 (42), or to be stabilized and accumulate in early and late endosomes/lysosomes (20) or to be destabilized (21). In our experimental setting, proBACE1 and BACE1 amounts are not altered by the substitution of the ubiquitination site, either in the basal situation or during proteasome or lysosome inhibition, suggesting that BACE1 ubiquitination is not involved in the control of its degradation and therefore that BACE1 and proBACE1 undergo ubiquitin-independent degradation. Such a degradation process was already described for other proteins (43, 44). The localization of proBACE1 in ESP implies that its degradation is regulated of by

processes controlling protein degradation in ER: i.e. ER(L)AD pathways (18, 19), which are known to be triggered by ER stress. Inhibition of ER(L)AD pathways increases ER stress, likely by creating a protein overload in ER. Interestingly, the ER stress inducer A23187 increases the amount of proBACE1, suggesting that in our study the unfolded protein response is not sufficient to restore adequate proteostasis of proBACE1. More importantly, this result shows that ER stress may be a trigger for disruption of proBACE1 proteostasis. We confirm, as previously described (45–47), that *O*-GlcNacylation, ubiquitination and ER stress are increased in the liver of mouse models of diabetes and we further show that these abnormalities accompany an increase in the amount of proBACE1 and total BACE1. Our interpretation is that during diabetes, hyperglycemia enhances *O*-GlcNacylation which reduces ER(L)AD (both contributing to ER stress), allowing the abnormal accumulation of proBACE1 in ESP which promotes the proBACE1-dependent cleavage of IR precursor. Aminosterol compound Claramine and its analogue Trodusquemine are PTP1B inhibitors (48, 49) that prevent IR dephosphorylation, keeping it in its activated state. Our results confirm that Claramine increases IR phosphorylation and signaling. Interestingly, IGF1R phosphorylation which is also controlled by PTP1B (50) is not increased by Claramine, which suggests that Claramine has very special properties resulting in a “specific” increase in IR phosphorylation. Of the aminosterols tested, only Claramine increases IR cell surface expression and this implies its ability to inhibit IR cleavage by BACE1. Interestingly, Claramine also reduces the BACE1-dependent cleavages of APP and APP<sub>swe</sub> (that are efficiently cleaved by proBACE1) but does not seem to impact NRG1 cleavage (that is poorly

cleaved by proBACE1), suggesting that Claramine alters proBACE1 biology. Claramine reduces the amount of proBACE1 in ESP. As this effect is particularly pronounced when proteasome is inhibited, we propose that it is due to Claramine's ability to increase the autophagy. However, this increased autophagy alone cannot fully explain the selective reduction of proBACE1 amount. Indeed, Claramine does not affect all the proteins over-represented in ESP, as shows its lack of effect on proIR. Moreover, the autophagy inducer Resveratrol (26) does not reduce the amount of proBACE1. Claramine increases the amount of proBACE1 in the Golgi apparatus, suggesting that it increases the efficiency of proBACE1 trafficking from the ESP to the Golgi apparatus. Genetic alterations of autophagic process in mice revealed that autophagy reduction in the liver participates to insulin resistance development (51–53). Our view (see above) is that reduced autophagy is one of the triggers for the cleavage of proIR by proBACE1, which worsens insulin resistance (12). In this context, Claramine through its abilities to increase autophagy, to reduce the cleavage of IR by BACE1 and to inhibit PTP1B could be a high potential compound to improve the liver insulin sensitivity. As a matter of fact, Claramine has already shown its efficacy to improve glycemic control in diabetic mice (49, 54). The properties of Claramine also make it an attractive molecule in the fight against AD. Indeed, BACE1 (55) and defects in autophagy (56) are involved in AD pathogenesis and PTP1B inhibitors are considered a promising strategy to combat a variety of AD-related detrimental processes (57). It then appears necessary to better delineate the biological effects of Claramine and to elucidate its mechanisms of action.

In summary, we characterized the sequence of events leading to the cleavage of IR by BACE1 in the liver during diabetes. We identified Claramine as an efficient antagonist of proBACE1-dependent cleavage of proIR with modes of action compatible with its use as a hepatic insulin sensitizer.

### **Experimental procedures**

**Chemicals** – DAPT and dec-RVKR-cmk were from Merck (Nottingham, UK). DON, OSMI-1, PUGNAc, glucosamine, insulin, heparin agarose, A23187, LY294002 and IGF2 were from Sigma Aldrich (Saint-Quentin Fallavier, France). Bafilomycin A1, MG-132, PR-619, Leupeptin, E-64-d and pepstatin-A were from Santa Cruz Biotechnology (Santa Cruz, CA, USA).

**Antibodies** - Antibodies for IR (C-19 for  $\beta$ -subunit and H-78 for  $\alpha$ -subunit), anti-phosphorylated IR (Tyr<sup>1162/1163</sup>) that also detects phosphorylated IGF1R (Tyr<sup>1135/1136</sup>), BACE1 (61-3E7), GRP78 (76-E6), O-GlcNac (CTD110.6), HA-probe (Y-11) and c-Myc (9E10) antibodies were from Santa Cruz Biotechnology. Golgin 97 monoclonal antibody (CDF4) was from (ThermoFisher scientific). Antibodies for  $\beta$ -actin (13E5), GAPDH (D4C6R), Ubiquitin (P4D1), K63- and 48-linkage specific polyubiquitin (D7A11 and D9D5) and LC3 were from Cell Signaling Technology (Danvers, MA, USA). BACE1 prodomain antibody (26-45) was from Genscript (Piscataway, NJ, USA). Anti-FlagM2 was from Sigma Aldrich. IGF1R antibody (NBP2-24885) was from Novus Biologicals (Centennial, CO, USA). Human IR Alexa Fluor 488-conjugated Antibody (clone 243522), used in flow cytometry experiments, and Human BACE1 ELISA kit were from R&D Systems (Minneapolis, MN, USA).

**Expression vectors** - Expression vectors for human NRG1 and APP were from OriGene Technologies (Rockville, MD, USA). Expression vector for HA-SUMO1<sub>Q94P</sub> was a gift from G. Salvesen (Addgene plasmid # 48965), Ubiquitin-Flag and IGF1R expression vectors were from K.L. Lim (Lee Kong Chian School of Medicine, Singapore) and R. O'Connor (University College Cork, Cork, Ireland), respectively. *EGR1* promoter-luciferase reporter vector was from J. L. Jameson (Northwestern University, Chicago, USA). Expression vectors for IR, IR<sub>FY/KK</sub>, IR<sub>Y3F</sub>, IR $\beta$  N-terminally fused to Gaussia luciferase, furin, EK-4, HA-tagged BACE1 inactive BACE1<sub>D289A</sub> were previously described (12). Mutated forms of BACE1 and IR and APP<sup>swe</sup> (the Swedish mutation K595N/M596L) were created using the GeneArt site-directed mutagenesis system (Thermo Fisher Scientific, Illkirch, France) or In-fusion cloning system (Takara Bio, Saint Germain en Laye, France).

**Cell culture and transfection** - HEK293 cells (Griptide 293 MSR) were from Thermo Fisher Scientific. HepG2 cell lines were from ATCC. Cells were maintained in culture as described by the manufacturers. No mycoplasma contamination was detected in any of the cultures. Transfection were performed with PolyJet reagent (SignaGen Laboratories, Rockville, MD, USA), as specified by the manufacturers.

**Mice** - Male *db/db* (*BKS.Cg-m<sup>+/+</sup>Leprdb/J*) and *db/+* (*BKS.Cg-m<sup>+/-</sup>Leprdb/J*) mice (Charles River Laboratories; Saint Germain Nuelles, France) were 10 weeks old at the time of killing. Liver was removed and pieces were snap frozen for ulterior analysis. Ten weeks old male C57Bl/6 mice (Charles River Laboratories; Saint Germain Nuelles, France) were randomly fed either a standard-fat diet (70% kcal

carbohydrate, 10% kcal fat, 20% kcal protein, 3.68 kcal g<sup>-1</sup>, Special Diet Services, Witham, UK) or a HFD (20% kcal carbohydrate, 60% kcal fat, 20% kcal protein, 5.13 kcal g<sup>-1</sup>) for 16 weeks before killing. Blood and tissues were collected as described above. Experiments were performed at Aix Marseille University (France) in accordance to the European directive 2010/63/EU on the protection of animals used for scientific purposes and approved by the "Comité d'éthique en expérimentation animale de Marseille."

**Enzymatic deglycosylation** - N-linked carbohydrate residues were removed by incubating cell lysates for 2 h at 37 °C with 1000 units of endoglycosidase H (EndoH) as described by the manufacturer (New England Biolabs, Beverly, MA, USA). Samples were then separated by SDS-PAGE and analyzed by western blotting.

**Subcellular fractionation** - The fractionation was performed using iodixanol gradient (Sigma-Aldrich). HepG2 cells were cultured for 36 hours in the presence of 25 mM glucose and treated with 10  $\mu$ M DAPT for the last 17 hours then washed and scraped in homogenization buffer [0.25 M sucrose, 10 mM Hepes, pH 7.4, 25 mM KCl, 2mM MgCl<sub>2</sub>, 1mM EDTA, protease inhibitor cocktail] and homogenized by 15 strokes through a 26-gauge needle syringe. The homogenate was centrifuged at 1000 g for 10 min to obtain post-nuclear supernatant (PNS). The PNS was further centrifuged at 10 000 g for 10 min to obtain post-mitochondrial (PMS) supernatant. The PMS was further centrifuged at 100 000 g for 2 hours and the resulting membrane pellet was suspended in 1.6 ml of homogenization buffer containing 25% (w/v) iodixanol. The vesicle suspension was layered underneath a gradient consisting of 1.6 ml of 20%, 15%, 10% and

5% iodixanol solutions. Gradient were centrifuged using a SW41Ti rotor at 50 000 g for 18h then 500 µl fractions were collected.

**Immunoblot** - Cells were lysed in the presence of a cocktail of protease and phosphatase inhibitor. PUGNAc (100 µM) or PR-619 (100 µM) were added in the lysis buffer for the study of O-GlcNacylation or Ubiquitination, respectively. Identical amounts of total protein were heat-denatured and reduced (70 °C; 10 min) then submitted to SDS-PAGE separation on 4-12% gradient or 12% NuPAGE gels (Thermo Fisher Scientific) and transferred to polyvinylidene fluoride membranes. Membranes were blocked for 1 h in 5% BSA solution and incubated with the appropriate primary and HRP-conjugated secondary antibodies (1:1000 and 1:10,000 dilutions, respectively). Immunodetections were performed using ECL reagent and image acquisition was performed by using a chemiluminescent CCD imager ImageQuant LAS 4000 (GE Healthcare, Velizy-Villacoublay, France). Densitometric analysis of the bands was performed with the ImageQuant TL software.

**Flow cytometry** - Cell surface expression of overexpressed IR was analyzed by flow cytometry (BD Accuri C6; BD Biosciences, San Jose, CA, USA). Cells were gated on forward and side scatter to exclude dead cells, debris and aggregates.

**Real-time PCR analysis** - Total RNA was extracted using Nucleospin RNA Kit (Macherey-Nagel, Hoerd, France), cDNA was synthesized from 0.5 µg of RNA using M-MLV reverse transcriptase (Thermo Fisher Scientific) and used for PCR amplification. RT-PCR were performed on the LightCycler 480 instrument (Roche

Applied Science, Meylan, France) using the Eva Green MasterMix (Euromedex, Souffelweyersheim, France). The comparative Ct method ( $2^{-\Delta\Delta CT}$ ) was used to calculate the relative differences in mRNA expression. The acidic ribosomal phosphoprotein P0 was used as housekeeping gene. Primers sequences are available upon request. Changes were normalized to the mean of control values, which were set to 1.

**Reporter assays** - For gene reporter assays, HEK293 cells were transfected with SV40-driven Renilla luciferase vector along with *EGR1* promoter-driven Firefly luciferase in addition to BACE1 and IR expression vectors. Firefly and Renilla luciferase were measured in cell lysates after addition of proper Genofax reagents (Yelen, Ensues la Redonne, France) using a luminometer (EnSight Multimode plate reader; Perkin Elmer, Waltham, MA, USA). Activities were calculated as the ratio Firefly/Renilla luciferase and expressed as fold change compared to control. IR-cleavage reporter assay was previously described (12). For luminescence-based Autophagy reporter assay, HepG2 cells were transiently transfected with the autophagy LC3-HiBiT Reporter vector (Promega, GA2550) encoding a fusion protein consisting of human LC3B, a N-terminal 11 amino acid HiBiT tag, and a connecting spacer that enhances reporter specificity for the autophagic pathway. Compounds to be tested were added at least 36 hours after transfection for a duration of 6 h (Bafilomycin A1) or 17 h (Claramine), then LC3-HiBiT reporter activity was measured using the Nano-Glo HiBiT Lytic Detection System (Promega, N3040). A decrease in LC3-HiBiT reporter activity reflects autophagic LC3 degradation and serves as a measure of autophagy induction while an increased

LC3-HiBiT reporter activity indicates autophagy inhibition.

**Transmission Electron microscopy** - After 5 minutes of wash with 0.1 M sodium cacodylate 587 buffer, cells were directly fixed in solution with glutaraldehyde 2.5% in 0.1 M sodium 588 cacodylate buffer during 1h at room temperature, then 3 times washed for 5 minutes with 589 0.1 M cacodylate buffer. Specimens were post-fixed with 2% osmium tetroxyde in 0.1 M 590 sodium cacodylate buffer during 1 h, then washed again 3 times for 10 minutes with 0.1 M 591 sodium cacodylate buffer. Progressive dehydration with 50% to 100% ethanol bath before 592 starting embedding in Low-Viscosity-Embedding Epoxy resin (SPURR) kit from 33% to 100% 593 SPURR. Cells were transferred from wells to tube before polymerization of resin overnight 594 at 72°C. Ultrathin 60 nm sections were obtained using Ultracut-E ultramicrotome (Reichert595 Jung, Southbridge, Massachusetts, USA) and contrast was performed using Uranyl acetate 596 and lead citrate solution. Pictures were obtained using JEM 1400 transmission electron 597 microscope (JEOL, Tokyo,

Japan) at 80kV with Megaview III Camera under iTEM Five 598 software (SIS Imaging, Münster, Germany).

**Statistical analyses** - All the experiments have been repeated at least three times. Data were analyzed with GraphPad Prism software and individual statistical two-sided tests used are identified in the figure legends. P-values  $\leq 0.05$  were considered statistically significant.

**Data availability:** Sequences of primers are available upon request (corresponding author). All remaining data are contained within the article.

**Acknowledgements:** We thank JF. Landrier, J. Astier and C. Couturier for providing mouse liver samples.

**Funding:** Institut national de la santé et la recherche médicale (Inserm).

**Conflict of interest:** The authors declare that they have no conflicts of interest with the contents of this article.

## References

1. Boucher, J., Kleinridders, A., and Kahn, C. R. (2014) Insulin receptor signaling in normal and insulin-resistant states. *Cold Spring Harb Perspect Biol.* 10.1101/cshperspect.a009191
2. Dev, R., Bruera, E., and Dalal, S. (2018) Insulin resistance and body composition in cancer patients. *Ann. Oncol.* **29**, ii18–ii26
3. Vella, V., Milluzzo, A., Scalisi, N. M., Vigneri, P., and Sciacca, L. (2018) Insulin Receptor Isoforms in Cancer. *Int J Mol Sci.* 10.3390/ijms19113615
4. Neth, B. J., and Craft, S. (2017) Insulin Resistance and Alzheimer's Disease: Bioenergetic Linkages. *Front Aging Neurosci.* **9**, 345
5. Pomytkin, I., Costa-Nunes, J. P., Kasatkin, V., Veniaminova, E., Demchenko, A., Lyundup, A., Lesch, K.-P., Ponomarev, E. D., and Strekalova, T. (2018) Insulin receptor in the brain: Mechanisms of activation and the role in the CNS pathology and treatment. *CNS Neurosci Ther.* **24**, 763–774
6. Haeusler, R. A., McGraw, T. E., and Accili, D. (2018) Biochemical and cellular properties of insulin receptor signalling. *Nat. Rev. Mol. Cell Biol.* **19**, 31–44
7. Wang, Y., Zhou, H., Palyha, O., and Mu, J. (2019) Restoration of insulin receptor improves diabetic phenotype in T2DM mice. *JCI Insight.* 10.1172/jci.insight.124945
8. Nagarajan, A., Petersen, M. C., Nasiri, A. R., Butrico, G., Fung, A., Ruan, H.-B., Kursawe, R., Caprio, S., Thibodeau, J., Bourgeois-Daigneault, M.-C., Sun, L., Gao, G., Bhanot, S., Jurczak, M. J., Green, M. R., Shulman, G. I., and Wajapeyee, N. (2016) MARCH1 regulates insulin sensitivity by controlling cell surface insulin receptor levels. *Nat Commun.* **7**, 12639
9. Song, R., Peng, W., Zhang, Y., Lv, F., Wu, H.-K., Guo, J., Cao, Y., Pi, Y., Zhang, X., Jin, L., Zhang, M., Jiang, P., Liu, F., Meng, S., Zhang, X., Jiang, P., Cao, C.-M., and Xiao, R.-P. (2013) Central role of E3 ubiquitin ligase MG53 in insulin resistance and metabolic disorders. *Nature.* **494**, 375–379
10. Choi, E., Zhang, X., Xing, C., and Yu, H. (2016) Mitotic Checkpoint Regulators Control Insulin Signaling and Metabolic Homeostasis. *Cell.* **166**, 567–581
11. Schmidt, V., Schulz, N., Yan, X., Schürmann, A., Kempa, S., Kern, M., Blüher, M., Poy, M. N., Olivecrona, G., and Willnow, T. E. (2016) SORLA facilitates insulin receptor signaling in adipocytes and exacerbates obesity. *J. Clin. Invest.* **126**, 2706–2720
12. Meakin, P. J., Mezzapesa, A., Benabou, E., Haas, M. E., Bonardo, B., Grino, M., Brunel, J.-M., Desbois-Mouthon, C., Biddinger, S. B., Govers, R., Ashford, M. L. J., and Peiretti, F. (2018) The beta secretase BACE1 regulates the expression of insulin receptor in the liver. *Nat Commun.* **9**, 1306
13. Creemers, J. W., Ines Dominguez, D., Plets, E., Serneels, L., Taylor, N. A., Multhaup, G., Craessaerts, K., Annaert, W., and De Strooper, B. (2001) Processing of beta-secretase by furin and other members of the proprotein convertase family. *J. Biol. Chem.* **276**, 4211–4217
14. Benjannet, S., Elagoz, A., Wickham, L., Mamrabachi, M., Munzer, J. S., Basak, A., Lazure, C., Cromlish, J. A., Sisodia, S., Checler, F., Chrétien, M., and Seidah, N. G. (2001) Post-translational processing of beta-secretase (beta-amyloid-converting enzyme) and its ectodomain shedding. The pro- and transmembrane/cytosolic domains affect its cellular activity and amyloid-beta production. *J. Biol. Chem.* **276**, 10879–10887
15. Kara, I., Poggi, M., Bonardo, B., Govers, R., Landrier, J.-F., Tian, S., Leibiger, I., Day, R., Creemers, J. W. M., and Peiretti, F. (2015) The paired basic amino acid-cleaving enzyme 4 (PACE4) is involved in the maturation of insulin receptor isoform B: an opportunity to reduce the specific insulin receptor-dependent effects of insulin-like growth factor 2 (IGF2). *J. Biol. Chem.* **290**, 2812–2821
16. Ortiz-Meoz, R. F., Jiang, J., Lazarus, M. B., Orman, M., Janetzko, J., Fan, C., Dubeau, D. Y., Tan, Z.-W., Thomas, C. J., and Walker, S. (2015) A small molecule that inhibits OGT activity in cells. *ACS Chem. Biol.* **10**, 1392–1397
17. Beckman, M., Holsinger, R. M. D., and Small, D. H. (2006) Heparin activates beta-secretase (BACE1) of Alzheimer's disease and increases autocatalysis of the enzyme. *Biochemistry.* **45**, 6703–6714

18. Fregno, I., and Molinari, M. (2019) Proteasomal and lysosomal clearance of faulty secretory proteins: ER-associated degradation (ERAD) and ER-to-lysosome-associated degradation (ERLAD) pathways. *Crit. Rev. Biochem. Mol. Biol.* **54**, 153–163
19. Fujita, E., Kouroku, Y., Isoai, A., Kumagai, H., Misutani, A., Matsuda, C., Hayashi, Y. K., and Momoi, T. (2007) Two endoplasmic reticulum-associated degradation (ERAD) systems for the novel variant of the mutant dysferlin: ubiquitin/proteasome ERAD(I) and autophagy/lysosome ERAD(II). *Hum. Mol. Genet.* **16**, 618–629
20. Kang, E. L., Biscaro, B., Piazza, F., and Tesco, G. (2012) BACE1 protein endocytosis and trafficking are differentially regulated by ubiquitination at lysine 501 and the Di-leucine motif in the carboxyl terminus. *J. Biol. Chem.* **287**, 42867–42880
21. Bao, J., Qin, M., Mahaman, Y. A. R., Zhang, B., Huang, F., Zeng, K., Xia, Y., Ke, D., Wang, Q., Liu, R., Wang, J.-Z., Ye, K., and Wang, X. (2018) BACE1 SUMOylation increases its stability and escalates the protease activity in Alzheimer's disease. *Proc. Natl. Acad. Sci. U.S.A.* **115**, 3954–3959
22. Ding, W.-X., Ni, H.-M., Gao, W., Hou, Y.-F., Melan, M. A., Chen, X., Stolz, D. B., Shao, Z.-M., and Yin, X.-M. (2007) Differential Effects of Endoplasmic Reticulum Stress-induced Autophagy on Cell Survival. *J. Biol. Chem.* **282**, 4702–4710
23. Blanchet, M., Borselli, D., Rodallec, A., Peiretti, F., Vidal, N., Bolla, J.-M., Digiorgio, C., Morrison, K. R., Wuest, W. M., and Brunel, J. M. (2018) Claramines: A New Class Of Broad-Spectrum Antimicrobial Agents With Bimodal Activity. *ChemMedChem.* **13**, 1018–1027
24. Petiot, A., Ogier-Denis, E., Blommaert, E. F., Meijer, A. J., and Codogno, P. (2000) Distinct classes of phosphatidylinositol 3'-kinases are involved in signaling pathways that control macroautophagy in HT-29 cells. *J Biol Chem.* **275**, 992–998
25. Blommaert, E. F., Krause, U., Schellens, J. P., Vreeling-Sindelárová, H., and Meijer, A. J. (1997) The phosphatidylinositol 3-kinase inhibitors wortmannin and LY294002 inhibit autophagy in isolated rat hepatocytes. *Eur J Biochem.* **243**, 240–246
26. Kou, X., and Chen, N. (2017) Resveratrol as a Natural Autophagy Regulator for Prevention and Treatment of Alzheimer's Disease. *Nutrients.* 10.3390/nu9090927
27. Huse, J. T., Liu, K., Pijak, D. S., Carlin, D., Lee, V. M.-Y., and Doms, R. W. (2002) Beta-secretase processing in the trans-Golgi network preferentially generates truncated amyloid species that accumulate in Alzheimer's disease brain. *J. Biol. Chem.* **277**, 16278–16284
28. Westmeyer, G. G., Willem, M., Lichtenthaler, S. F., Lurman, G., Multhaup, G., Assfalg-Machleidt, I., Reiss, K., Saftig, P., and Haass, C. (2004) Dimerization of beta-site beta-amyloid precursor protein-cleaving enzyme. *J. Biol. Chem.* **279**, 53205–53212
29. Zhang, F., Su, K., Yang, X., Bowie, D. B., Paterson, A. J., and Kudlow, J. E. (2003) O-GlcNAc modification is an endogenous inhibitor of the proteasome. *Cell.* **115**, 715–725
30. Keembiyehetty, C. N., Krzeslak, A., Love, D. C., and Hanover, J. A. (2011) A lipid-droplet-targeted O-GlcNAcase isoform is a key regulator of the proteasome. *J. Cell. Sci.* **124**, 2851–2860
31. Rahman, M. A., Hwang, H., Cho, Y., and Rhim, H. (2019) Modulation of O-GlcNAcylation Regulates Autophagy in Cortical Astrocytes. *Oxid Med Cell Longev.* **2019**, 6279313
32. Wani, W. Y., Ouyang, X., Benavides, G. A., Redmann, M., Cofield, S. S., Shacka, J. J., Chatham, J. C., Darley-Usmar, V., and Zhang, J. (2017) O-GlcNAc regulation of autophagy and  $\alpha$ -synuclein homeostasis; implications for Parkinson's disease. *Mol Brain.* **10**, 32
33. Kocaturk, N. M., and Gozuacik, D. (2018) Crosstalk Between Mammalian Autophagy and the Ubiquitin-Proteasome System. *Front Cell Dev Biol.* **6**, 128
34. Costantini, C., Ko, M. H., Jonas, M. C., and Puglielli, L. (2007) A reversible form of lysine acetylation in the ER and Golgi lumen controls the molecular stabilization of BACE1. *Biochem. J.* **407**, 383–395
35. Qing, H., Zhou, W., Christensen, M. A., Sun, X., Tong, Y., and Song, W. (2004) Degradation of BACE by the ubiquitin-proteasome pathway. *FASEB J.* **18**, 1571–1573
36. Singh, A. K., and Pati, U. (2015) CHIP stabilizes amyloid precursor protein via proteasomal degradation and p53-mediated trans-repression of  $\beta$ -secretase. *Aging Cell.* **14**, 595–604

37. Koh, Y. H., von Arnim, C. A. F., Hyman, B. T., Tanzi, R. E., and Tesco, G. (2005) BACE is degraded via the lysosomal pathway. *J. Biol. Chem.* **280**, 32499–32504
38. Zhang, M., Deng, Y., Luo, Y., Zhang, S., Zou, H., Cai, F., Wada, K., and Song, W. (2012) Control of BACE1 degradation and APP processing by ubiquitin carboxyl-terminal hydrolase L1. *J. Neurochem.* **120**, 1129–1138
39. Clague, M. J., and Urbé, S. (2010) Ubiquitin: same molecule, different degradation pathways. *Cell.* **143**, 682–685
40. Komander, D., and Rape, M. (2012) The ubiquitin code. *Annu. Rev. Biochem.* **81**, 203–229
41. Zhang, L., Xu, M., Scotti, E., Chen, Z. J., and Tontonoz, P. (2013) Both K63 and K48 ubiquitin linkages signal lysosomal degradation of the LDL receptor. *J. Lipid Res.* **54**, 1410–1420
42. Kang, E. L., Cameron, A. N., Piazza, F., Walker, K. R., and Tesco, G. (2010) Ubiquitin regulates GGA3-mediated degradation of BACE1. *J. Biol. Chem.* **285**, 24108–24119
43. Erales, J., and Coffino, P. (2014) Ubiquitin-independent proteasomal degradation. *Biochim. Biophys. Acta.* **1843**, 216–221
44. Opoku-Nsiah, K. A., and Gestwicki, J. E. (2018) Aim for the core: suitability of the ubiquitin-independent 20S proteasome as a drug target in neurodegeneration. *Transl Res.* **198**, 48–57
45. Ruan, H.-B., Han, X., Li, M.-D., Singh, J. P., Qian, K., Azarhoush, S., Zhao, L., Bennett, A. M., Samuel, V. T., Wu, J., Yates, J. R., and Yang, X. (2012) O-GlcNAc Transferase/Host Cell Factor C1 Complex Regulates Gluconeogenesis by Modulating PGC-1 $\alpha$  Stability. *Cell Metab.* **16**, 226–237
46. Otda, T., Takamura, T., Misu, H., Ota, T., Murata, S., Hayashi, H., Takayama, H., Kikuchi, A., Kanamori, T., Shima, K. R., Lan, F., Takeda, T., Kurita, S., Ishikura, K., Kita, Y., Iwayama, K., Kato, K., Uno, M., Takeshita, Y., Yamamoto, M., Tokuyama, K., Iseki, S., Tanaka, K., and Kaneko, S. (2013) Proteasome Dysfunction Mediates Obesity-Induced Endoplasmic Reticulum Stress and Insulin Resistance in the Liver. *Diabetes.* **62**, 811–824
47. Yamagishi, N., Ueda, T., Mori, A., Saito, Y., and Hatayama, T. (2012) Decreased expression of endoplasmic reticulum chaperone GRP78 in liver of diabetic mice. *Biochem. Biophys. Res. Commun.* **417**, 364–370
48. Krishnan, N., Konidaris, K. F., Gasser, G., and Tonks, N. K. (2018) A potent, selective, and orally bioavailable inhibitor of the protein-tyrosine phosphatase PTP1B improves insulin and leptin signaling in animal models. *J. Biol. Chem.* **293**, 1517–1525
49. Qin, Z., Pandey, N. R., Zhou, X., Stewart, C. A., Hari, A., Huang, H., Stewart, A. F. R., Brunel, J. M., and Chen, H.-H. (2015) Functional properties of Claramine: a novel PTP1B inhibitor and insulin-mimetic compound. *Biochem. Biophys. Res. Commun.* **458**, 21–27
50. Blanquart, C., Boute, N., Lacasa, D., and Issad, T. (2005) Monitoring the activation state of the insulin-like growth factor-1 receptor and its interaction with protein tyrosine phosphatase 1B using bioluminescence resonance energy transfer. *Mol. Pharmacol.* **68**, 885–894
51. Zhang, K. (2018) “NO” to Autophagy: Fat Does the Trick for Diabetes. *Diabetes.* **67**, 180–181
52. Yang, L., Li, P., Fu, S., Calay, E. S., and Hotamisligil, G. S. (2010) Defective hepatic autophagy in obesity promotes ER stress and causes insulin resistance. *Cell Metab.* **11**, 467–478
53. Yamamoto, S., Kuramoto, K., Wang, N., Situ, X., Priyadarshini, M., Zhang, W., Cordoba-Chacon, J., Layden, B. T., and He, C. (2018) Autophagy Differentially Regulates Insulin Production and Insulin Sensitivity. *Cell Rep.* **23**, 3286–3299
54. Dodd, G. T., Xirouchaki, C. E., Eramo, M., Mitchell, C. A., Andrews, Z. B., Henry, B. A., Cowley, M. A., and Tiganis, T. (2019) Intranasal Targeting of Hypothalamic PTP1B and TCPTP Reinstates Leptin and Insulin Sensitivity and Promotes Weight Loss in Obesity. *Cell Rep.* **28**, 2905-2922.e5
55. Lane, C. A., Hardy, J., and Schott, J. M. (2018) Alzheimer’s disease. *Eur. J. Neurol.* **25**, 59–70
56. Cao, J., Zhong, M. B., Toro, C. A., Zhang, L., and Cai, D. (2019) Endo-lysosomal pathway and ubiquitin-proteasome system dysfunction in Alzheimer’s disease pathogenesis. *Neurosci. Lett.* **703**, 68–78
57. Vieira, M. N. N., Lyra E Silva, N. M., Ferreira, S. T., and De Felice, F. G. (2017) Protein Tyrosine Phosphatase 1B (PTP1B): A Potential Target for Alzheimer’s Therapy? *Front Aging Neurosci.* **9**, 7

## Figure legends

**Figure 1: proBACE1 interacts with proIR.** HA-BACE1 and FLAG-IR overexpressed in HEK293 cells were detected by immunoblot (IB) using anti-HA, anti-BACE1 prodomain (PRO) and anti-FLAG antibodies in (a) cell lysates and (b) after immunoprecipitation (IP) of HA-BACE1 or FLAG-IR using the corresponding anti-tag antibodies. (c) HA-BACE1 was immunoprecipitated (IP: HA) from lysates of cells expressing HA-BACE1 alone or with furin (FUR) then BACE1 and proBACE1 were detected. (d) HA-BACE1 and/or FLAG-BACE1 were expressed as indicated then BACE1 was detected in cell lysates and after FLAG-BACE1 immunoprecipitation (IP: FLAG); right panel: long exposure of the blot. (e) HA-BACE1 and/or IR were expressed as indicated then BACE1 and IR were detected, in cell lysates and after HA-BACE1 immunoprecipitation. Positions of: IR precursor (proIR); BACE1 dimer (d); proBACE1 (p); mature BACE1 (m); heavy chain immunoglobulin (\*) are indicated.

**Figure 2: proBACE1 cleaves proIR in the early secretory pathway.** Wild-type (WT), inactive (D289A) or PC-resistant (R42G) forms of BACE1 were overexpressed with IR or its indicated mutated forms. (a) proBACE1, total BACE1 and IR $\alpha$  subunit were detected in cell lysates, IR<sub>SOL</sub> was detected in conditioned media. (b) Cells were treated with DAPT (10  $\mu$ M, 17 hours) then IR $\beta$  subunit and BACE1 were detected in cell lysates. (c) Cells were treated with DAPT then IR $\beta$  and IR $\alpha$  subunits were detected in cell lysates. (d) IR $\alpha$  subunit and IR<sub>SOL</sub> were detected in cell lysates and in conditioned media, respectively. (e) Cell lysates were treated with EndoH and IR $\alpha$  subunit was detected. (f) BACE1 and IR expressing cells were treated with Dec-RVKR-CMK (RV; 20  $\mu$ M, 17 hours) or transfected with EK4 expression vector (EK) to inhibit PC then IR<sub>SOL</sub> was detected in the conditioned media and IR $\beta$  subunit, proBACE1 and BACE1 were detected in cell lysates. (g) Distribution of IR, IR<sub>CTF</sub> and IR<sub>NTF</sub> in subcellular membrane vesicles of HEPG2 cells fractionated by iodixanol density gradient. Golgi apparatus- and ER-rich fractions are identified by the detection of Golgin 97 and GRP78, respectively. Positions of: IR precursor (proIR); IR C-terminal fragment (IR<sub>CTF</sub>); IR N-terminal fragment (IR<sub>NTF</sub>, black arrowhead), core glycosylated (co) and complex N-glycosylated (cx) proBACE1 are indicated.

**Figure 3: proBACE1 proteostasis is regulated by O-GlcNacylation-dependent degradations.** HA-BACE1 expressing cells were (a) cultured in conventional media (25 mM glucose) or incubated for 17 hours in low glucose media (LG; 5.5 mM glucose) in the absence or presence of glucosamine (GlcN; 1mM) then BACE1 was immunoprecipitated (IP: HA) and BACE1 and proBACE1 were detected, (b) treated for 17 hours with deoxynorleucine (DON; 5 mM), OSMI-1 (35  $\mu$ M) or incubated in low glucose media (LG) then total protein O-GlcNacylation (O-GlcNac), proBACE1, BACE1 and  $\beta$ -actin (loading control) were detected in cell lysates, (c) left untreated (cont) or treated for 17 hours with inhibitors of lysosome-dependent degradation: E-64-d (E; 10  $\mu$ M) + pepstatin (P; 20  $\mu$ M), E + P + leupeptine (L; 20  $\mu$ M), NH<sub>4</sub>Cl (20 mM), Bafilomycin A1 (BAF; 30 nM) or with inhibitors of proteasome-dependent degradation: MG132 (MG; 1 $\mu$ M) or PR-619; (10  $\mu$ M), then proBACE1 was detected. The positive autophagy marker LC3II and total Ubiquitin were detected to control the efficacy of the inhibitors. Coomassie blue staining of the gels confirms that comparable amounts of proteins were analyzed. (d) Cells expressing BACE1 and IR were treated with Bafilomycin A1, MG132 or OSMI-1 then proBACE1, BACE1 and IR $\beta$  subunit were detected. (e) HEK293 cells were transfected with empty plasmid (EV) or BACE1 expressing vector, HepG2

cells were treated for 17 hours with Bafilomycin A1 (BAF; 30 nM) then proBACE1 was detected in cell lysates and in heparin-agarose bound fraction. Positions of: BACE1 dimer (d); proBACE1 (p); mature BACE1 (m); heavy chain immunoglobulin (\*); IR precursor (proIR) are indicated.

**Figure 4: proBACE1 is degraded by ubiquitin-independent pathway.** Cells were transfected with expression vectors coding for the wild-type (WT) or ubiquitination-deficient (K501R) BACE1 and for ubiquitin (Ubi-FLAG). (a) detection of BACE1 (HA), proBACE1 (PRO) and ubiquitin (FLAG) in cell lysates. (a) immunoprecipitation of BACE1 (IP: HA) or ubiquitin (IP: FLAG) followed by the detection (IB) of total ubiquitin (FLAG, Ubi), K48- and K63-linked polyubiquitin chains (UbiK48, UbiK63), proBACE1 (PRO) and BACE1. (c) Cells expressing the indicated forms of BACE1 were treated for 17 hours with Bafilomycin A1 (BAF; 30 nM) or MG132 (MG; 1  $\mu$ M) then proBACE1 and BACE1 were detected in cell lysate. (d) Cells expressing IR and the indicated forms of BACE1 were treated as in (c) in the presence of DAPT and IR $\beta$  subunit was detected in cell lysate. (e) same as (d) but without DAPT treatment, IR<sub>SOL</sub> and IR $\beta$  subunit were detected in the conditioned media and in cell lysates, respectively. Positions of: IR precursor (proIR); IR C-terminal fragment (IR<sub>CTF</sub>); BACE1 dimer (d); heavy chain immunoglobulin (\*) are indicated.

**Figure 5: proBACE1 degradation and ER stress are functionally connected.** Cells expressing BACE1 were treated for 17 hours with Bafilomycin A1 (BAF; 30 nM) or MG132 (MG; 1  $\mu$ M) along with OSMI-1 (35  $\mu$ M) as indicated. (a) total ubiquitination (Ubi), proBACE1, BACE1, GRP78 and total protein content (Coomassie staining) were detected in cell lysates (d indicates the position of BACE1 dimer). (b) mRNA levels of ER stress markers GRP78, CHOP and spliced XBP1 (sXBP1) were measured by RT-PCR. BACE1 overexpressing cells were treated for 17 hours with A23187 (A23; 1  $\mu$ M) or MG132 (MG; 1  $\mu$ M), then (c) mRNA levels of the indicated ER stress markers were measured by RT-PCR and (d) proBACE1 and BACE1 were detected in cell lysates. Data are means  $\pm$  s.d. Statistical analyses analyses were made using Anova followed by Dunnett's (panel a) or *t*-test (panel c): \*\*\*p < 0.001.

**Figure 6: O-GlcNacylation, ubiquitination and ER stress are increased in livers of *db/db* mice.** (a) O-GlcNacylation (O-GlcNac), total ubiquitination (Ubi) and  $\beta$ -actin (loading control) were detected by immunoblot in lysates of liver from standard fat diet fed mice (SFD) and high fat diet fed mice (HFD); a densitometric analysis of the signals is shown (lower panel). (b) O-GlcNacylation, total ubiquitination, proBACE1, GRP78 and  $\beta$ -actin were detected in lysates of liver from *db/+* and *db/db* mice; a densitometric analysis of the signals is shown (lower panel). (c) mRNA levels of the indicated ER stress markers were measured by RT-PCR, in livers from SDF and HFD fed mice. (d) BACE1 was measured by ELISA in lysates of liver from *db/+* and *db/db* mice (same amount of protein was used). Values are expressed as fold over the means of the control mice. Data are means  $\pm$  s.d. Statistical analyses was made using Mann-Whitney (panels a, b and d) or *t*-test (panel c): \* p < 0.05, \*\*p < 0.01, \*\*\*p < 0.001.

**Figure 7: Claramine reduces BACE1-dependent cleavage of IR.** (a) HEK293 cells expressing IR and wild-type (WT) or inactive (D289A) BACE1 were treated with Claramine (Clara; 10  $\mu$ M, 17 hours), then cell surface IR was measured by flow cytometry. Data are means  $\pm$  s.d of median fluorescence intensities corrected for the value obtained with cells transfected with

the empty vector and expressed relative to the control situation (set at 1). **(b)** HEK293 cells expressing BACE1 and IR were treated with Claramine (Clara) in the presence of DAPT and IR $\beta$  subunit was detected in cell lysates. **(c)** Same as **(a)** except that IR<sub>SOL</sub> was detected in the conditioned media; densitometric analysis of the signals was performed (lower panel), values are expressed relative to the mean in the control situation. **(d)** HEK293 Cells expressing BACE1 were treated with Claramine (Clara), Bafilomycin A1 (BAF) or MG132 (MG), then proBACE1 and total BACE1 were detected in cell lysates. **(e)** HepG2 cells transfected with LC3-HiBiT reporter were treated for 17 hours with the indicated concentrations of Claramine (Clara) or with Bafilomycin A1 (BAF; 20 nM; 6 hours) as positive control for autophagy inhibition. Data are means  $\pm$  s.d of reporter activity measured as LC3-HiBiT luminescence normalized to untreated situation. **(f)** Detection of LC3 and  $\beta$ -actin (loading control) in HepG2 cells treated with Claramine, densitometric analysis of the signals was performed (lower panel), values are expressed relative to the mean in the control situation. **(g)** Detection by transmission electron microscopy of autophagosome-like structures (multimembranous autophagic vacuoles) in HepG2 cells treated with Claramine. The area outlined in red in the image is enlarged in the following image the white bar at the bottom right of each micrograph corresponds to 1  $\mu$ M. **(h)** HEK293 cells expressing BACE1 were treated for 17 hours with LY294002 (LY; 10  $\mu$ M) or Bafilomycin A1 (BAF, 30 nM) then proBACE1, total BACE1 and LC3 and  $\beta$ -actin (loading control) were detected in cell lysates. Statistical analyses were made using *t*-test (panels **a** and **f**) or Anova followed by Dunnett's (panel **e**): \*\**p* < 0.01, \*\*\**p* < 0.001.

**Figure 8: Diagram summarizing the mechanisms that regulate IR cleavage by BACE1.** proBACE1 cleaves proIR in the early secretory pathway (ESP). The amount of proBACE1 in ESP is regulated by its degradation (involving ER(L)AD and autophagy) and trafficking through the secretory pathway. Diabetes increases O-GlcNacylation, which reduces proBACE1 degradation. As a result, proBACE1 accumulates in ESP where it cleaves proIR. Claramine, increases autophagy and stimulates the trafficking of proBACE1 to the Golgi apparatus, which reduces the amount of proBACE1 in the ESP thereby decreasing proIR cleavage.

Figure 1

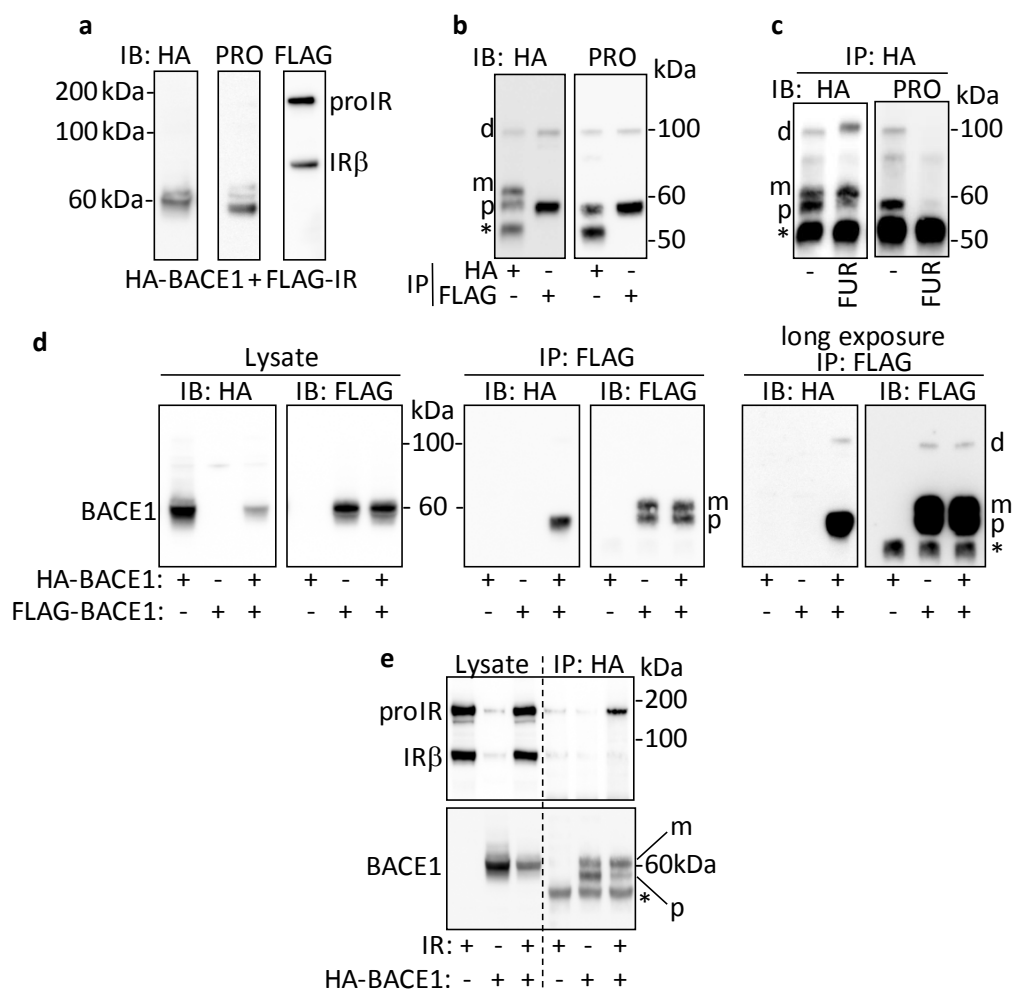


Figure 2

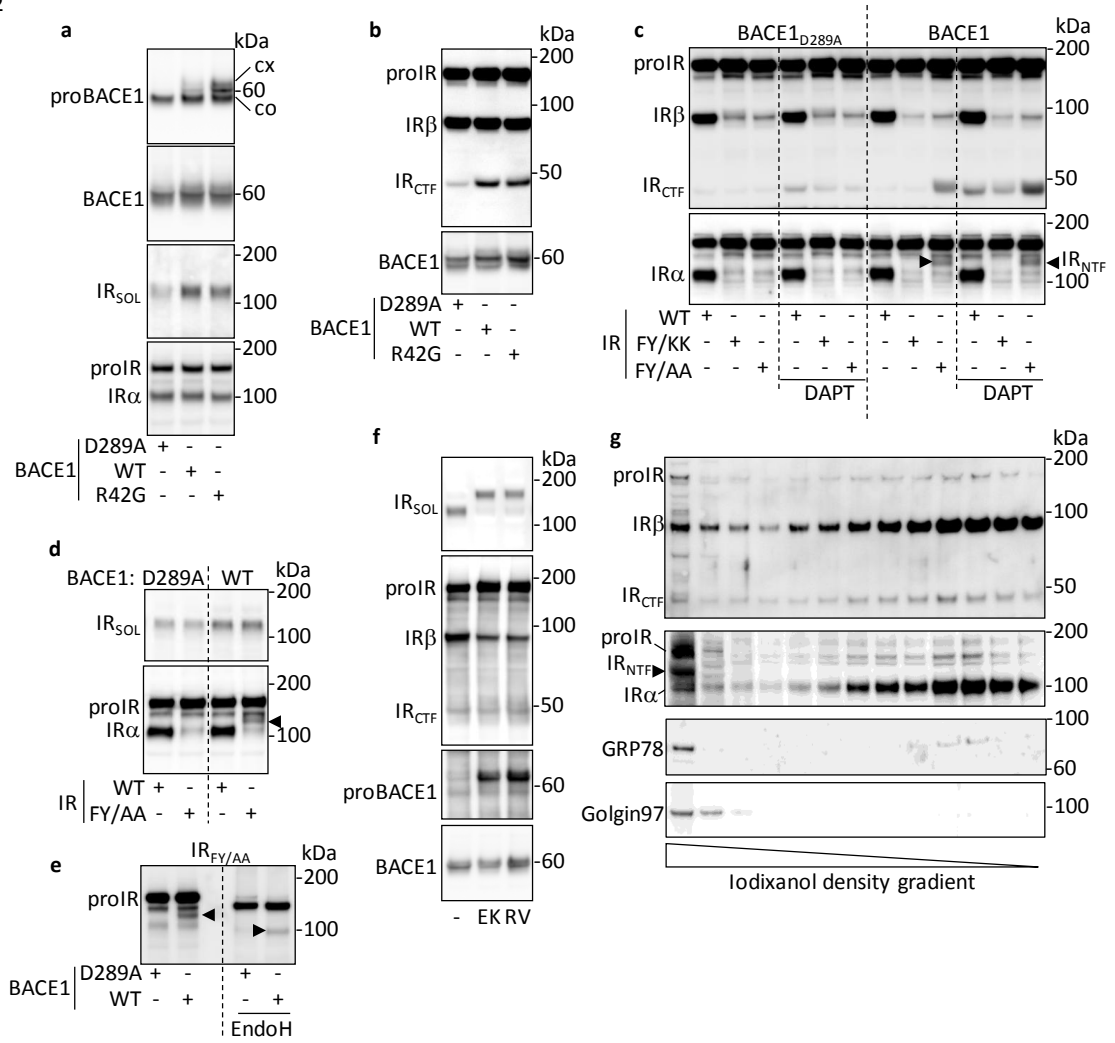


Figure 3

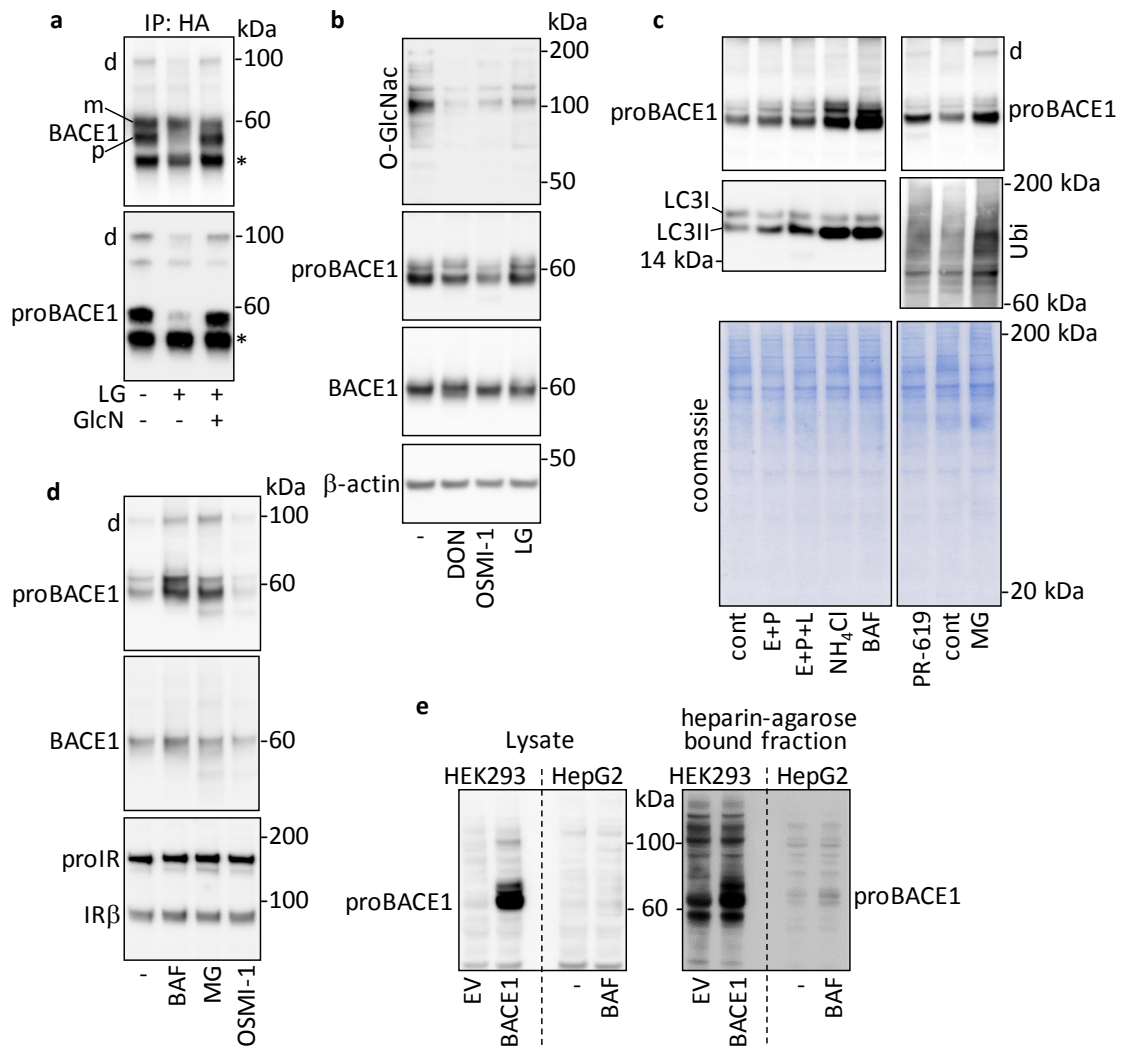


Figure 4

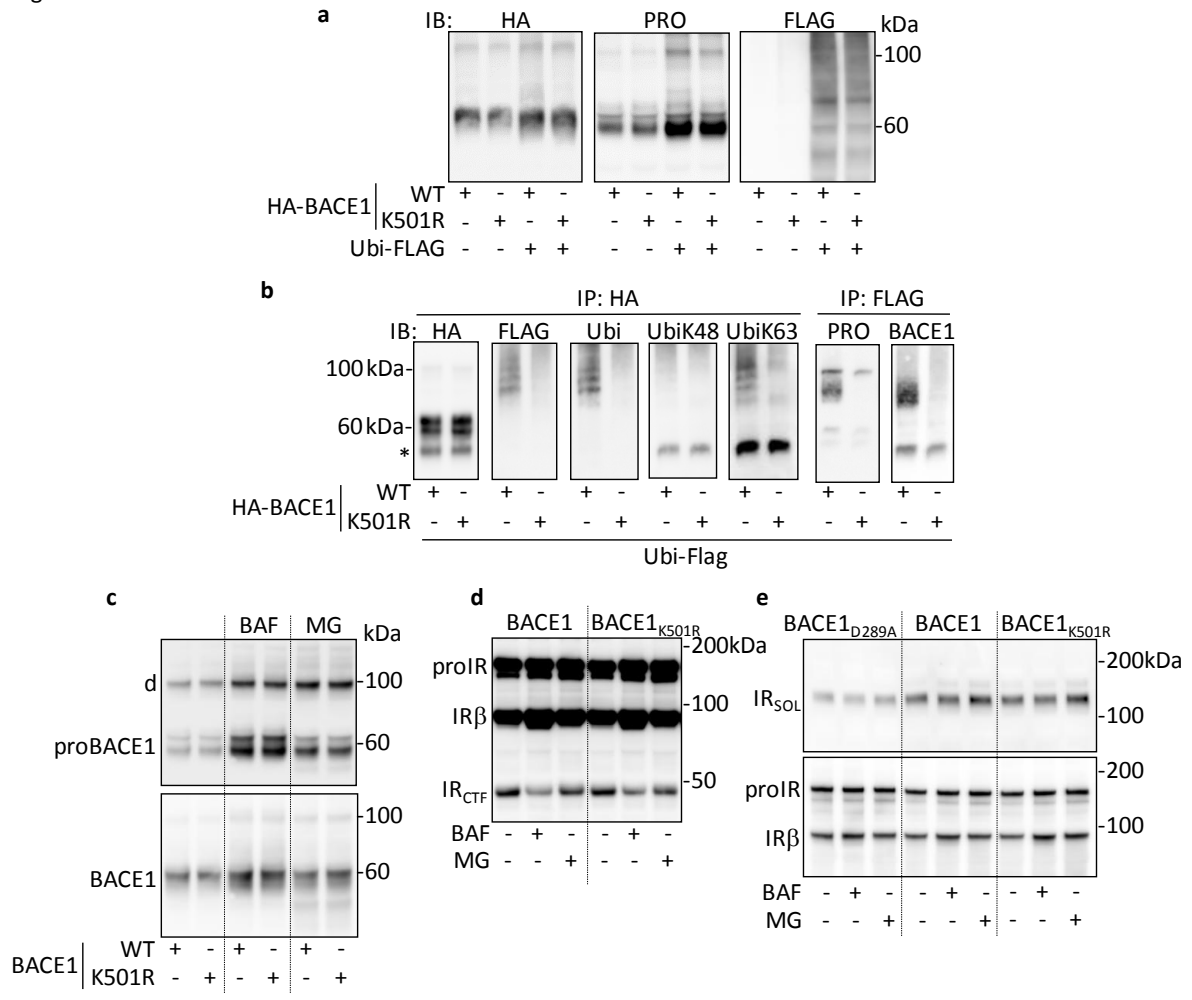


Figure 5

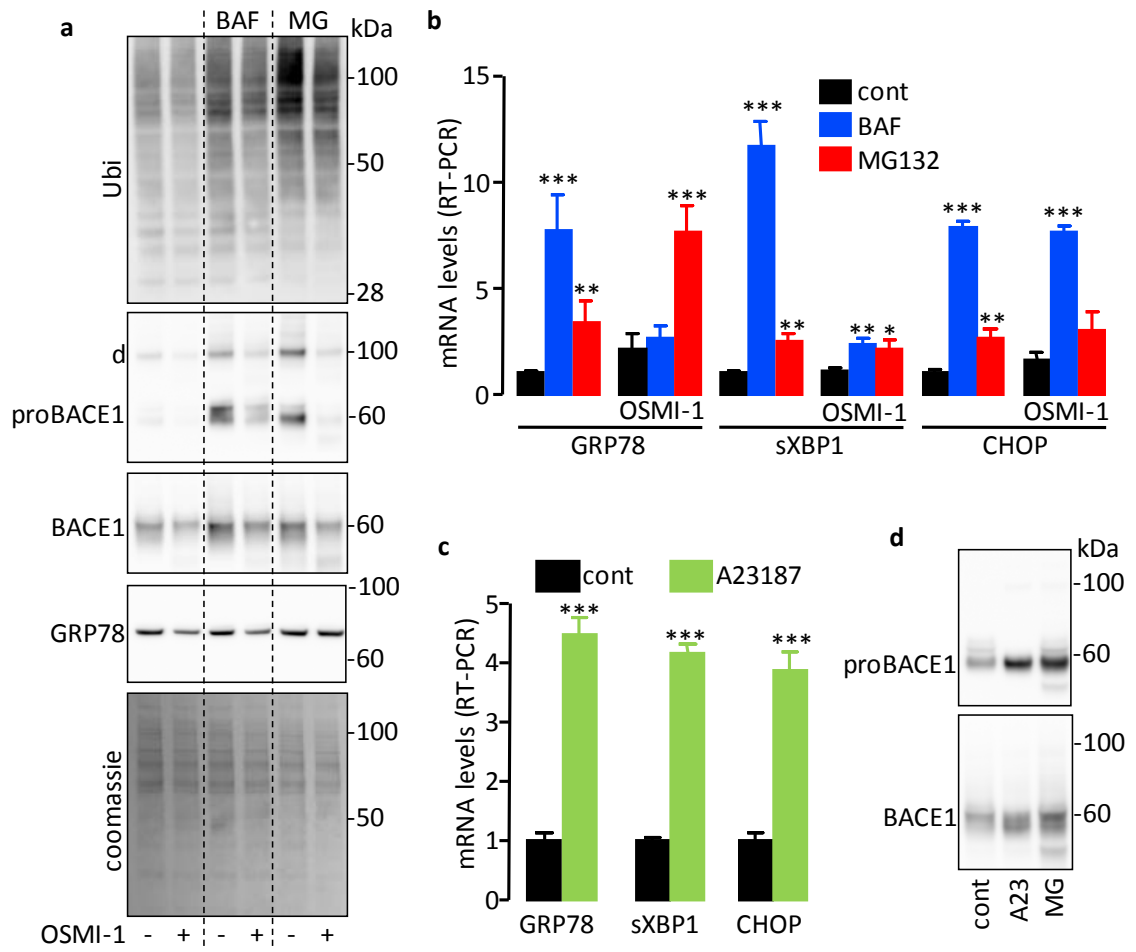


Figure 6

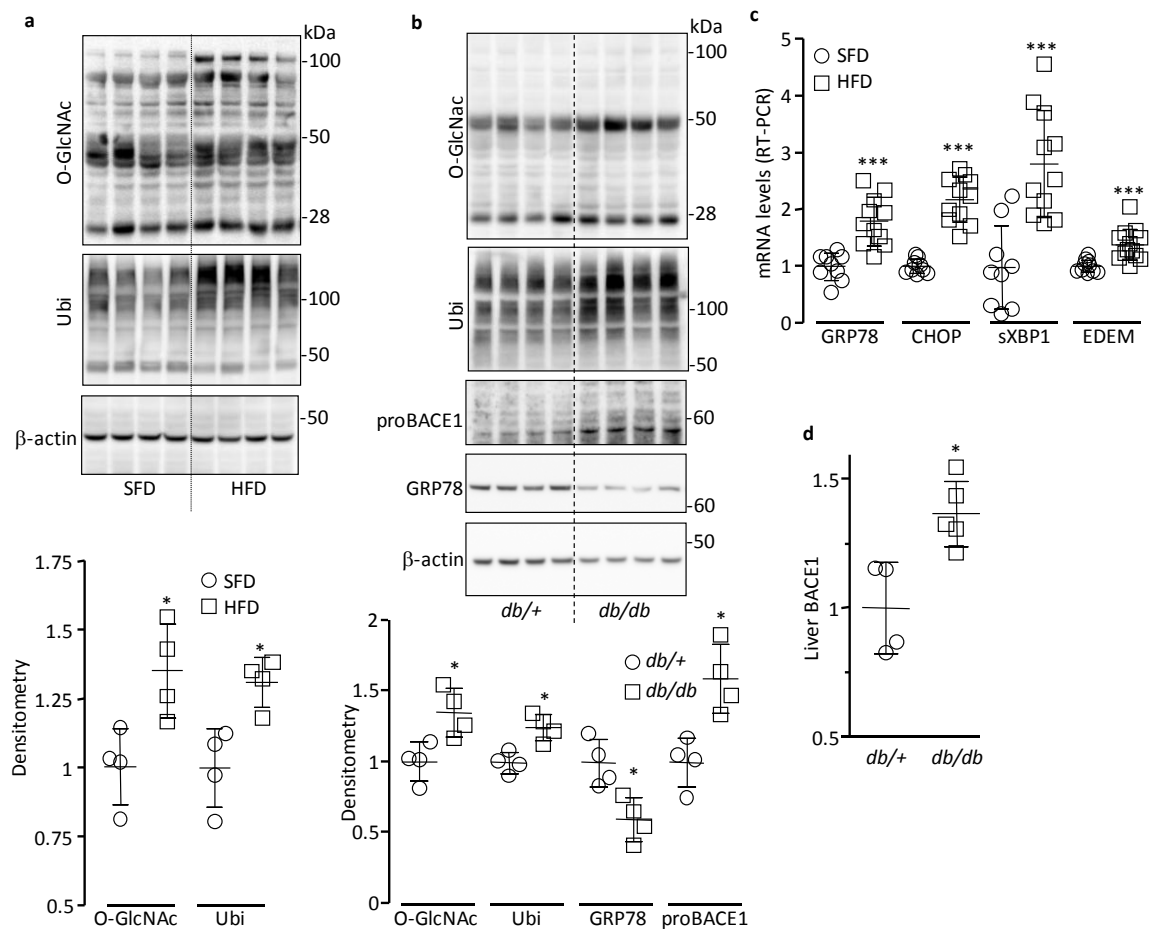


Figure 7

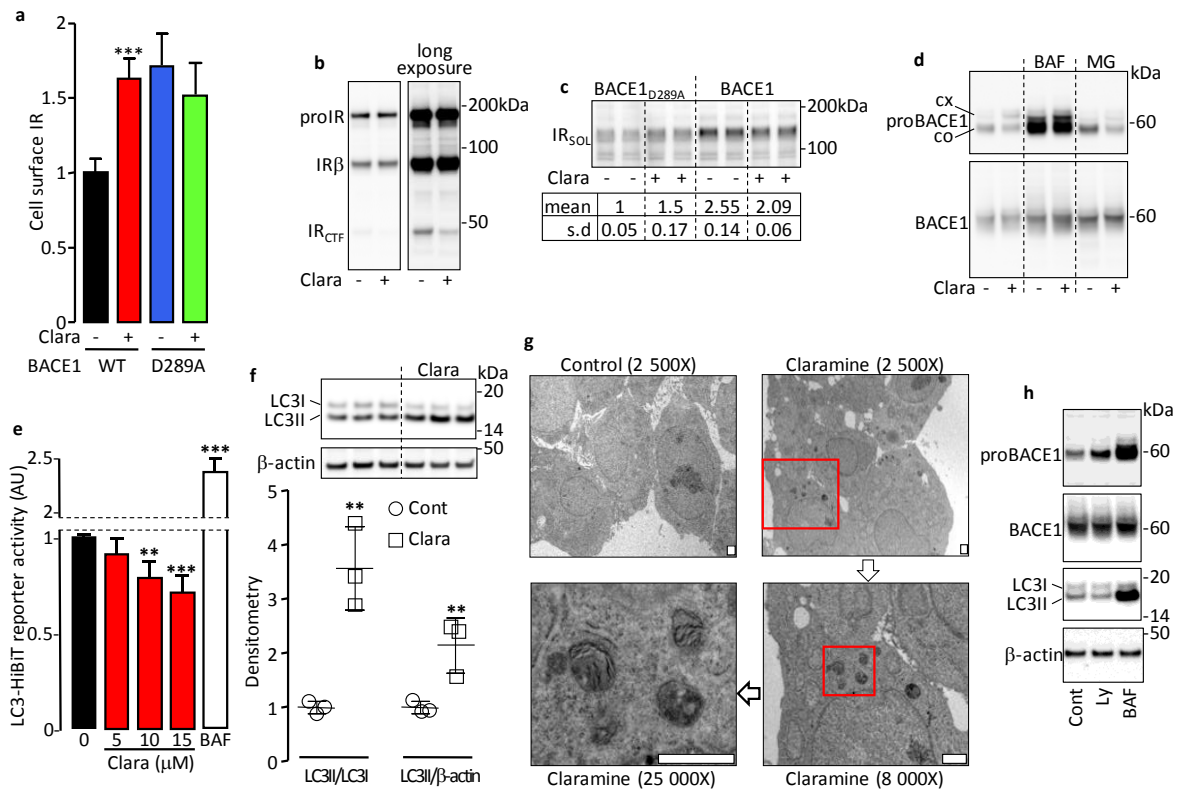


Figure 8

